

Adding color: Visualization of energy landscapes in spin glasses

Katja Biswas¹ and Helmut G. Katzgraber²

¹*Department of Physics and Astronomy, Texas A&M University, College Station, Texas 77843-4242, USA*

²*Microsoft Quantum, Redmond, Washington 98052, USA*

Disconnectivity graphs are used to visualize the minima and the lowest energy barriers between the minima of complex systems. They give an easy and intuitive understanding of the underlying energy landscape and, as such, are excellent tools for understanding the complexity involved in finding low-lying or global minima of such systems. We have developed a classification scheme that categorizes highly-degenerate minima of spin glasses based on similarity and accessibility of the individual states. This classification allows us to condense the information pertained in different dales of the energy landscape to a single representation using color to distinguish its type and a bar chart to indicate the average size of the dales at their respective energy levels. We use this classification to visualize disconnectivity graphs of small representations of different tile-planted models of spin glasses. An analysis of the results shows that different models have distinctly different features in the total number of minima, the distribution of the minima with respect to the ground state, the barrier height and in the occurrence of the different types of minimum energy dales.

PACS numbers: 75.50.Lk, 75.40.Mg, 05.50.+q, 64.60.-i

I. INTRODUCTION

Originally introduced to describe energy landscapes of tetrapeptides [1], disconnectivity graphs have become a powerful tool in visualizing the complex relationships between the different energy minima of bio-polymers and nano-cluster [2–4]. Disconnectivity graphs represent a complex multi-dimensional energy landscape via a set of minima and the connections between them. The connections illustrate the lowest energy barrier a system has to overcome to be able to transition between different minima. In this respect, the disconnectivity graphs give a clear visual aid and may also serve as a tool in understanding some of the difficulties when dealing with the optimization of complex systems and processes. Moreover, with the insights gained, bespoke nontrivial random benchmark problems can be designed to benchmark optimization tools both classical [5–10] and quantum [11–16].

In spin glasses complexity originates from the interplay of frustration and disorder [17–19], and can have an effect on the dynamics and success rates of optimization routines. Trying to gain an understanding of the underlying energy structures of spin glasses has a recurring history. Garstecki *et al.* [20] used enumeration to draw disconnectivity graphs and dynamical connectivity graphs for small two-dimensional Ising spin systems. Amoruso *et al.* [21] used a hierarchical approach to calculate minimum energy barriers. Burda *et al.* used the lid algorithm for the barriers [22] and a steepest descent method to find internal structures [23]. The branch and bound algorithm was used to gain information about the energy landscape for spin systems up to the third excitation [24]. Dall and Sibani [25] used aging dynamics to gain some insight into the structure of valleys and barriers of the energy landscape of Ising spin glasses. Barrier trees [26, 27] have been used to describe p -spin models. Seyed-Allaei *et al.* [28] used disconnectivity graphs to study the energy-landscape of up to 27 spin Ising models. Finally, Zhou *et al.* [29, 30] utilized random walks to obtain minima and barriers and thus produce disconnectivity graphs.

Minimum-energy configurations that have regions of spins

for which the local Hamiltonian is zero, broaden the minima and form dales (wide valleys) of equal energy in the energy landscape. For larger systems, these dales [31] add difficulties to the visualization of disconnectivity graphs as they essentially consist of a vast number of minima connected via their own energy and thus do add very little to an intuitive understanding of the underlying energy structure of the system. For this reason we propose to simplify the visualization of these structures by merging them into representations that we refer to as “dale minima.” We further distinguish between different types of dale minima, which are then visualized via colors in the disconnectivity graph, and indicate their respective sizes by bar charts for the different energy levels. This greatly enhances the intuitive understanding of the underlying energy landscapes and simplifies the representations, allowing for the mapping of larger structures and higher energies while preserving the core information of the landscape. The idea of grouping minima has been utilized in the ballistic search method [32–35] to find ground-state configurations for various problems. In ballistic search, minima that are connected by a single variable or single spin flip at no energy cost are grouped into one general category which in Refs. [32–35] are called “clusters.” However, our approach is different in that we further distinguish between the different ways the minima can be connected.

A different approach to obtain information about ground states was given by Landry and Coppersmith [36] who define a cluster as groups of minima connected in a way analogous to the ballistic search method, but further distinguish between different structures that can occur within a cluster which they call a “bunch.” In their definition, a bunch is a local structure of spins that are either zero-energy spins or under certain fulfilled conditions can become zero-energy spins. In this way, a single configuration can have multiple bunches, which are then used to obtain information about the structure of the individual ground states. Our approach also differs from the aforementioned bunches in that, to ease the visualization, we use the overall connectivity between the individual minima. In other words, although the connection between minima is

influenced by local structures of spins within the particular minimum energy configurations, we are not interested in characterizing these local structures. We characterize the entire minimum to belong to a certain type which we call either a regular, or a dale minimum. This approach allows us to effectively enhance and reduce the visualization of minima in disconnectivity graphs, which is the main goal of this paper.

To demonstrate the visualization approach we propose in this work, we use our enhanced disconnectivity graphs to study the underlying energy landscape of instances of planar tile-planted spin glasses [37, 38]. These are special types of tunable spin glasses used to benchmark optimization techniques that have been constructed with a known ground-state solution. Note that other types of Ising Hamiltonians with planted solutions have been constructed on Chimera graphs [13, 39–41], using a random adaptive optimization method [42], as well as via patch planting [43].

The article is structured as follows. In section II A we introduce and explain our classification scheme. Section II B explains the basics of disconnectivity graph. Section III gives a short overview of the tile-planted spin glasses constructed with different elementary plaquettes and which we refer to as C_1 -type model, C_2 -type model, and C_3 -type model. In section IV we discuss our results, followed by conclusions.

II. METHODS

A. Classification

Disconnectivity graphs are two-dimensional representations of high-dimensional potential energy landscapes. In their simplest form, they depict the minima of the landscape and the lowest high-energy barriers between any two minima. The lowest high-energy barrier is the minimum increase in energy necessary to transition from one minimum to another. When dealing with disordered spin systems several factors are to be taken into account that complicate the generation of disconnectivity graphs.

For big enough systems of spin-glasses in which the spin-spin interactions are drawn from a discrete and finite distribution, there exist arrangements of the spin-spin interaction that allow some of the spins to take any orientation without changing the energy of the system. This is typically the case when the local interactions centered around a spin s_i and their corresponding connecting spins sum to zero, i.e. $H_{E_i} = 0$. We call the spins s_i which show this effect zero-energy spins, thus highlighting the fact that their contribution to the total energy of the system is zero. These effects can influence isolated spins or groups of connected spins. Furthermore, certain arrangements of spins and interactions can “transfer” the effects of zero local energy to other spins, thus leading to pathways in the energy landscape that can only be traversed in specific directions *without increasing the energy*. A different orientation of a single spin constitutes a different configuration of the whole system. Hence, configurations that only differ by spin orientations of the described form constitute dales in the energy landscape. A dale here is a region on the energy

landscape that has the same energy for different configurations of the system [44], i.e., the configurations are linked to each other by paths in the energy landscape that do not require an intermediate increase in energy. From a practical point of view when generating disconnectivity graphs, the minima belonging to the same dale increase the storage of data substantially while adding very little information to the energy structure of the system. In addition, dales clutter disconnectivity graphs with unnecessary information. From an energy connectivity perspective, one can think of each such a dale as an individual but degenerate state. This has led us to develop a color scheme for the disconnectivity graphs to distinguish between regular (nondegenerate) minima and various types of dales.

We distinguish between different types of minima. The types are based on similarity arguments and accessibility of the minima within the dales. We distinguish the minima as follows:

Regular minimum: A regular minimum is a minimum for which the flip of any spin of the system increases the energy.

Type-1 dale minimum: A dale minimum of type-1 is a degenerate minimum in which any combination of flips of the zero-energy spins preserves the energy of the system.

Type-2 dale minimum: A dale minimum of type-2 is a degenerate minimum in which only some, but not all, combinations of flips of the zero-energy spins preserve the energy of the system.

Type-3 dale minimum: A dale minimum of type-3 represents a connection of dale minima accessible only via specific transitions between the minima.

We further separate type-3 dale minima into two subcategories, which we call “type-3 dale minima with a simple path” and “type-3 dale minima with a split path.” These subcategories are based on the specific ways the energy landscape has to be traversed in order to preserve the energy of the system. Furthermore, note that the classification into regular minima, type-1 dale minima and type-2 dale minima is based on the overall connectivity of the individual configurations of the whole configuration space, i.e., while the zero-energy spins can form multiple small clusters within the systems, the classification according to the types is determined by the occurrence of the structures of connecting spins of the highest type. This is justified by the fact that these individual structures are the ones that determine the connectivity of the individual configurations on the configuration space. We also emphasize that the present study is performed for sparse graphs with fixed connectivity. A different, more complex, picture might emerge for Ising Hamiltonians on random, as well as fully-connected graphs.

In the disconnectivity graphs, we distinguish the different types of minima using colors. The regular minima are depicted in black, whereas type-1 and type-2 dale minima are colored in blue and green, respectively. Because type-3 dale

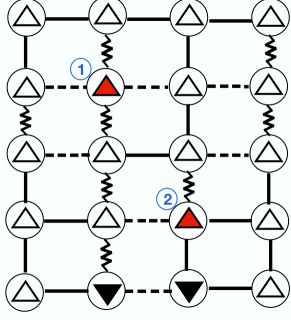


FIG. 1: Visualization of type-1 dale minima. The interactions $J_{ij} = -1, 1$, and 2 are represented by wiggly lines (\sim), dashed lines ($---$), and solid lines ($—$), respectively. White triangles \triangle represent spin up and black triangles \blacktriangledown represent spin down. The red triangles \triangle labeled ① and ② are zero-energy spins. These can be flipped in any combination at no energy cost.

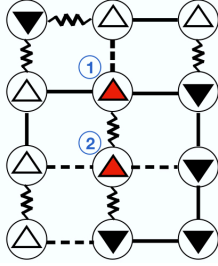


FIG. 2: Visualization of type-2 dale minima. The interactions $J_{ij} = -1, 1$, and 2 are represented by wiggly lines (\sim), dashed lines ($---$), and solid lines ($—$), respectively. White triangles \triangle represent spin up and black triangles \blacktriangledown represent spin down. The red triangles \triangle labeled ① and ② are zero-energy spins. They can be flipped only in certain combinations at no energy cost.

minima are two dales joined together, we represent them by connecting the corresponding dales by a horizontal line (colored in red) at their respective energies indicating the zero-energy transition between the two connecting dales.

Figures 1 to 6 illustrate via examples the different dale minima. Upward triangles represent Ising spins with the value $+1$ (up) and spins with the value -1 (down) are represented by downward-pointing triangles. Zero-energy spins are drawn in red. The interactions J_{ij} between spins i and j are drawn as solid lines when $J_{ij} = +2$, dashed when $J_{ij} = +1$, and wiggly lines when $J_{ij} = -1$. Note that the examples given in Figs. 1 to 6, only show the sections necessary to illustrate the different types of dale minima and are part of larger systems.

Figure 1 shows an example of a type-1 dale minimum. In this example, there are two zero-energy spins (red) As can be seen from the figure, any combination of the two zero-energy spins (spin 1 and spin 2) preserves the energy of the system. Without additional zero-energy spins such a minimum has a degeneracy of 4 originating from the free choice of orienta-

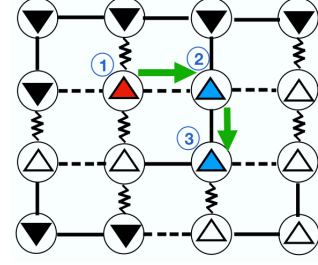


FIG. 3: Visualization of type-3 dale minima with a simple path. The interactions $J_{ij} = -1, 1$, and 2 are represented by wiggly lines (\sim), dashed lines ($---$), and solid lines ($—$), respectively. White triangles \triangle represent spin up and black triangles \blacktriangledown represent spin down. In the presented configuration only the red triangle \triangle labeled ① is a zero-energy spin and can be flipped at no energy cost. However, once spin ① has been flipped, the blue spin \triangle labeled as ② becomes a zero-energy spin. Lastly, only after ② flips the spin labeled ③ can be flipped at no energy cost. The direction of this simple path is indicated by the green arrows (\rightarrow).

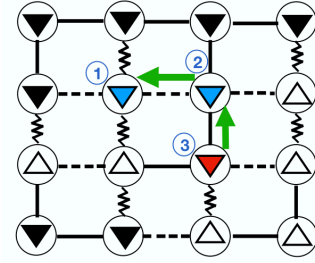


FIG. 4: Visualization of type-3 dale minima with a simple path in the reverse direction of Fig. 3. The interactions $J_{ij} = -1, 1$, and 2 are represented by wiggly lines (\sim), dashed lines ($---$), and solid lines ($—$), respectively. White triangles \triangle represent spin up and black triangles \blacktriangledown represent spin down. In the presented configuration only the red triangle \triangle labeled ③ is a zero-energy spin and can be flipped at no energy cost. However, once spin ③ has been flipped the blue spin \triangle labeled with ② becomes a zero-energy spin. And lastly, only after ② flips the spin labeled ① can be flipped at no energy cost. The direction of this simple path is indicated by the green arrows (\leftarrow). Note that this path is in the reverse direction of Fig. 3.

tion, i.e., both spins up ($\uparrow\uparrow$), only one of the spins up ($\uparrow\downarrow$ and $\downarrow\uparrow$) or both spins down ($\downarrow\downarrow$). In this example the free choice of flipping any combination of the zero-energy spins originates from their separation, i.e., that they are not nearest neighbors. Therefore, each choice of spin up or down does not affect the other, they are independent of each other.

In Fig. 2 a type-2 dale minimum is illustrated. Here the two zero-energy spins are nearest neighbors, which together with the arrangement of the spin-spin interactions leads to the following scenario: A flip of one spin influences the flipping of the other spin, i.e., if spin 1 is flipped then spin 2 will have negative local energy and thus can no longer be flipped without an increase in energy. Similarly, if spin 2 is flipped, then

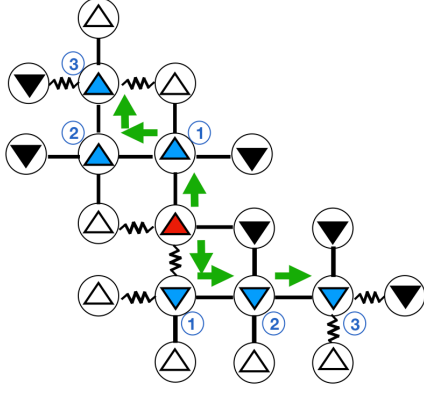


FIG. 5: Visualization of type-3 dale minima with a split path. The interactions $J_{ij} = -1, 1$, and 2 are represented by wiggly lines (\sim), dashed lines ($---$), and solid lines ($—$), respectively. White triangles \triangle represent spin up and black triangles \blacktriangledown represent spin down. In the configuration shown, only the red triangle \triangle is a zero-energy spin and can be flipped at no energy cost. Once the zero-energy spin has been flipped the spins drawn in blue \triangle \blacktriangledown which are labeled ① become zero-energy spins, and if ① have been flipped, the blue spins labeled ② can be flipped at no energy cost. This then allows to flip spin ③. Starting with flipping the center spin \triangle , this dale splits into two paths, indicated by the green arrows \rightarrow .

spin 1 will in its up-configuration be in a local minimum (has negative local energy) and can no longer be flipped. In this example the degeneracy originating from the zero-energy spin effects is 3, corresponding to the orientations of both spins up ($\uparrow\uparrow$) or only one of them up and the other down ($\uparrow\downarrow$ and $\downarrow\uparrow$). Note that in general, a necessary condition for the occurrence of this type of dale minimum is that at least two of the zero-energy spins have to be neighboring.

Figures 3 and 4 illustrate a type-3 dale minimum with a simple path. In Fig. 3 only spin 1 is a zero-energy spin. However, if spin 1 is flipped, then spin 2 becomes a zero-energy spin and can be flipped without an increase in energy. Further, if spin 1 and 2 are flipped, then spin 3 is a zero-energy spin and can be flipped at zero energy cost leading to the configuration depicted in Fig. 4. Conversely, if the system starts in a configuration of Fig. 4, then the order of the flipping of the spins is $3 \rightarrow 2 \rightarrow 1$, i.e., representing the spins in the order (1, 2, 3) the accessibility of the minima of this dale can be depicted as

$$\uparrow\uparrow\uparrow \longleftrightarrow \downarrow\uparrow\uparrow \longleftrightarrow \downarrow\downarrow\uparrow \longleftrightarrow \downarrow\downarrow\downarrow. \quad (1)$$

Note that, while each of the configurations in the schematic representation, Eq. (1), is a minimum on its own, each can only access a limited number of neighboring minima belonging to the same dale in the energy landscape. This means that the direct accessibility of the minima is dependent on the current minimum. The overall dale is pathway dependent. Pathway dependent in this example means that there are only two pathways (one in each direction) that connect all the minima belonging to the same dale minimum. In this example, the local degeneracy of the dale minimum is 4, representing the four subminima.

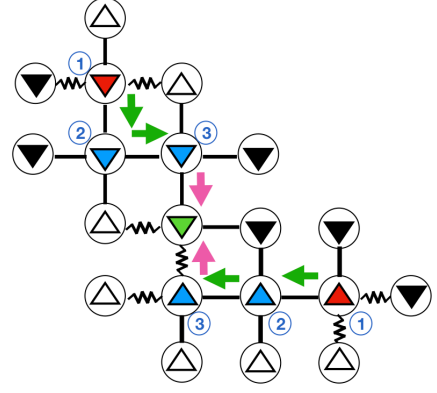
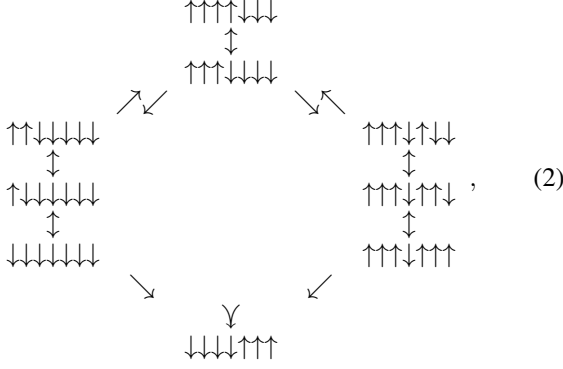


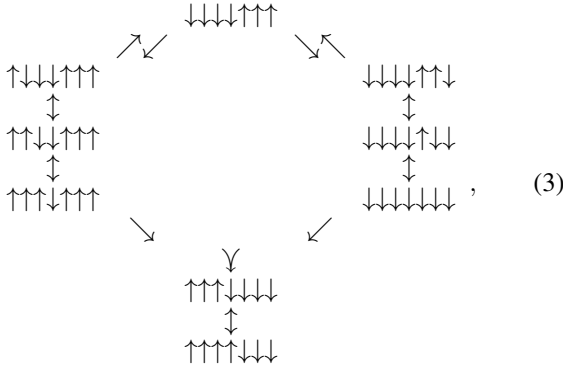
FIG. 6: Visualization of type-3 dale minima with a split path in the reverse direction of Fig. 5. The interactions $J_{ij} = -1, 1$, and 2 are represented by wiggly lines (\sim), dashed lines ($---$), and solid lines ($—$), respectively. White triangles \triangle represent spin up and black triangles \blacktriangledown represent spin down. In the configuration shown the two red triangles \triangle and \blacktriangledown labeled ① are zero-energy spins and can be flipped at no energy cost. Once they have been flipped the spins drawn in blue \triangle \blacktriangledown which are labeled ② become zero-energy spins, which if flipped allow the spins labeled ③ to be flipped at no energy cost. They form two paths, which are indicated by the green arrows \rightarrow . Only if both the paths have been completed, i.e., both the spins labeled ③ have been flipped, the center spin indicated in green \triangle can be flipped at zero energy cost. This double condition on the flippability of the center spin is indicated by the pink arrows \rightarrow .

Another variation of the type-3 dale minima is illustrated in Figs. 5 and 6. We call this subclass type-3 dale minimum with a split path, denoting that the transition between the two extreme minima (i.e., minima in Fig. 5 and minima in Fig. 6 in our example) do not follow a single path but rather a path that can be thought of to be split into two (or more) segments. A path here denotes a sequence of flipping of spins which are neighboring to each other. In the minima depicted in Fig. 5 only the center spin (drawn in red) is a zero-energy spin and can be flipped at no cost. However, once the center spin has been flipped it opens the two paths denoted by 1, 2, and 3, which can be either flipped in sequence or alternating between the two paths while maintaining the directional order. A flip of the zero-energy spin makes spin labeled 1 a zero-energy spin, which when flipped allows to flip spin number 2 and lastly spin number 3, if 2 has been flipped. This directional order has to be maintained in both directions in order for the transition to occur without an increase in energy. Flipping the spins along both the paths leads to the minimum depicted in Fig. 6. The reverse transition is shown in Fig. 6. Here the two outermost spins (depicted in red) are zero-energy spins and can be flipped at no cost. This allows then the flipping of the spins marked with 2 and 3 in subsequent order. Only after both of the paths have been completed, i.e., if both the spins marked with 3 are flipped, the center spin (drawn in green) becomes a zero-energy spin and can be flipped without an increase in energy. The resulting minima after all the spin flips have been completed is the minima depicted in Fig. 5. These transitions

can also be visualized as



representing schematically the transition corresponding to Fig. 5, and



representing schematically the transition depicted in Fig. 6. The wedged arrows denote the requirement that both of the preceding paths have to be completed before the next step. Note, that both the representations, Eq. (2) and Eq. (3), are simple representation of an underlying highly-dimensional nature, meaning that the transitions between the two outermost minima (the minima depicted in Fig. 5 and Fig. 6) have multiple possible realizations corresponding to a large variety of pathways across the dale in the energy landscape. Each step or point in the configuration space is a subminimum situated within the dale. The dale in our example is comprised of 17 subminima, where the two minima depicted in Fig. 5 and Fig. 6 are its outermost points that can only be accessed from one minimum but have two possible transitional minima for leaving in both the cases. The paths shown here have been selected based on their significance in highlighting the important aspects of the transitions.

B. Disconnectivity Graphs

In order to draw a disconnectivity graph, first, all the minima of the system have to be calculated. We do this via a complete enumeration of all possible spin configurations. Then, the height of the lowest energy barrier connecting the minima is calculated by considering the possible paths between the minima. For this purpose the procedure of Cieplack *et al.* [20]

for the calculation of possible pathways was followed. Further, to deal with the large number of minima in a computationally effective manner not all barriers [45] are calculated but an approximation is used. This approximation is based on the structural difference between the minima: For each minimum only the barriers to the nearest n minima are calculated. With nearest, we mean the number of differences in the orientation of the spins between any two minima and n is a given number of calculated barriers. We reason that when searching for low-energy pathways a system is likely to transition over intermediate minima or funnels of intermediate minima. This approximation greatly reduced the number of necessary barrier computations and thus allows for a complete mapping of the energy landscape to a disconnectivity graph. A similar approach was used in the analysis of potential energy landscapes of hexapeptides [46]. In general, the validity and the extent to which this approximation can be applied depends on the specific problem studied. We discuss this in more detail below in Sec. III.

Figures 7, 8, and 9 show examples of disconnectivity graphs obtained for the planted spin-glass models discussed below. The minima are represented by vertical bars, whose lowest points denote their energy. The branching points represent the lowest high-energy barrier needed to overcome to transition between the adjacent minima. The black bars represent regular minima, i.e., minima for which a flip of any spin would lead to an increase in energy. The blue bars represent type-1 dale minima, the green bars represent type-2 dale minima, and red horizontal lines joining two or more minima at the bottom indicate type-3 dale minima.

The minima are joined and sorted into cluster structures according to their energy barriers. Within each individual cluster, the minima are arranged based on the number of spins up. Minima with the highest number of spins up are drawn towards the left and sequentially minima with an increasing number of spins down are arranged toward the right [47].

To indicate the size of the different types of minima, i.e., the number of subminima belonging to the individual dales, we add a bar chart to the right-hand side of the disconnectivity graph. This chart is arranged such that the vertical axis represents the energies of the minima and dales, and the horizontal axis represents the average number of subminima belonging to the types, which we call the size of the types of minima.

III. MODEL

For the numerical experiments we focus on two-dimensional spin glasses on a square lattice with tile-planted solutions consisting of combinations of either C_1 , C_2 or C_3 unit cells, as shown in Fig. 10 Unit cell C_1 consists of one $J_{ij} = -1$ and three $J_{ij} = +2$ interactions between spins i and j that together form a square and on whose vertices the spins s_i are located. If all spins are either oriented in the up or all in the down configuration the local Hamiltonian of this configuration has ground-state energy $H_{C_1} = -5$. Unit cell C_2 consists of one $J_{ij} = -1$, one $J_{ij} = +1$ and two $J_{ij} = +2$ spin-spin interactions, which can be arranged in three distinct

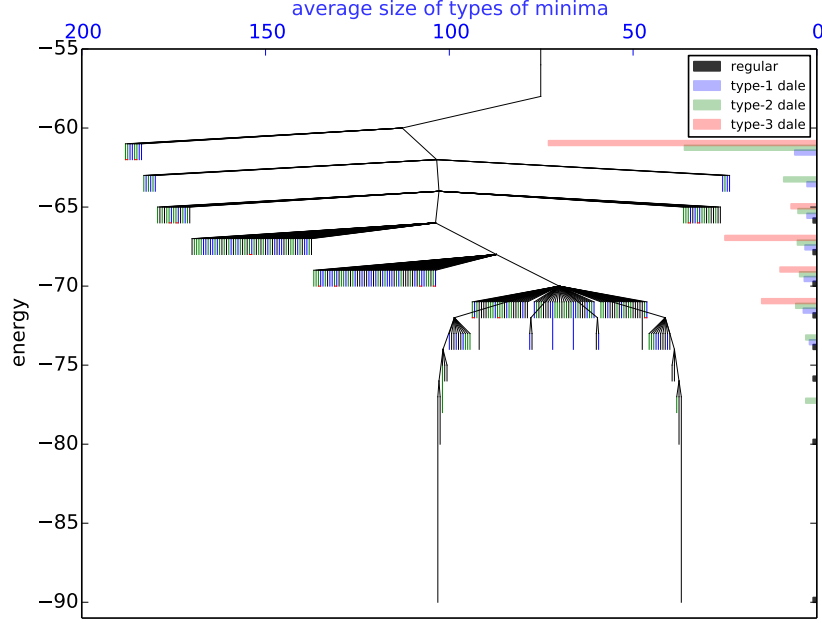


FIG. 7: Example of a disconnectivity graph for a planted spin-glass model (C_1 , see below) on a two-dimensional square lattice with $N = 36$ spins. The black vertical bars represent regular minima, the blue bars represent type-1 dale minima, the green bars represent type-2 dale minima and the red vertical bars indicate type-3 dale minima. The bar chart on the right shows the average size (i.e., the number of subminima comprising the dales) of the types of minima at their respective energy levels. The axis denoting the average size of types of minima only applies to the bar chart on the right-hand side of the disconnectivity graph. This axis does not represent the total number of minima in the system.

ways shown in Fig. 10. This unit cell has four ground state configurations with an energy $H_{C_2} = -4$. Unit cell C_3 has one $J_{ij} = -1$, two $J_{ij} = +1$ and one $J_{ij} = +2$ spin-spin interactions. Their possible arrangements are shown in Fig. 10. Unit cell C_3 has 6 ground states, corresponding to an energy of $H_{C_1} = -3$. The total system is constructed by placing the unit cells in a checker-board fashion such that only the vertices are joined, see Fig. 11. Within a subgroup C_1 , C_2 , or C_3 the unit cells are chosen and rotated randomly to form the larger system. Note that arranged in this way, the larger systems will have two known ground-state solutions, where all spins are either pointing up or all spins are pointing down. The total Hamiltonian is then given by the sum over all interactions J_{ij} centered around the individual spins

$$H = -\frac{1}{2} \sum_{\langle ij \rangle \in E} J_{ij} s_i s_j = \frac{1}{2} \sum_i H_{E_i} s_i. \quad (4)$$

In Eq. (4) the sum is taken over all vertices, $s_i = \pm 1$ denote the values of the individual spins in their up or down configurations, respectively, and H_{E_i} is the local Hamiltonian of the edges centered around spin i .

While some of the solutions of the ground states are constructed, each of these types represents a model of different complexity. The hardness in terms of time to solution (TTS) of pure and of mixed types of these models has been studied numerically in Refs. [37, 38]. In this work we map out the

underlying energy landscapes of these tile-planted systems.

IV. RESULTS

Results have been obtained for systems with $N = 6 \times 6$ spins, i.e., 18 unit cells. To obtain sufficient statistics for each of the C_1 , C_2 and C_3 types of planted spin glasses a sample of 100 systems is randomly generated and evaluated. The minima of the systems are obtained by complete enumeration and for each of the minima, barriers are calculated to the closest 80 minima. Although we only study one system size in this work, the obtained results should be qualitatively representative for the underlying behavior of the model system.

Figure 12 shows the distribution of the minimum hamming distance for the three models of planted spin glasses. The hamming distance here is understood as the minimum number of differences in the orientation of spins between two minima. For type-1 and type-2 dale minima, only the hamming distances between the two closest subminima are represented, i.e., between the subminima of each dale with the shortest hamming distance. To take into account the complexity in transitioning between the subminima belonging to type-3 dale minima, for this class only the hamming distances between the minima farthest apart on the energy landscape have been taken into account. Since for each of the models studied mul-

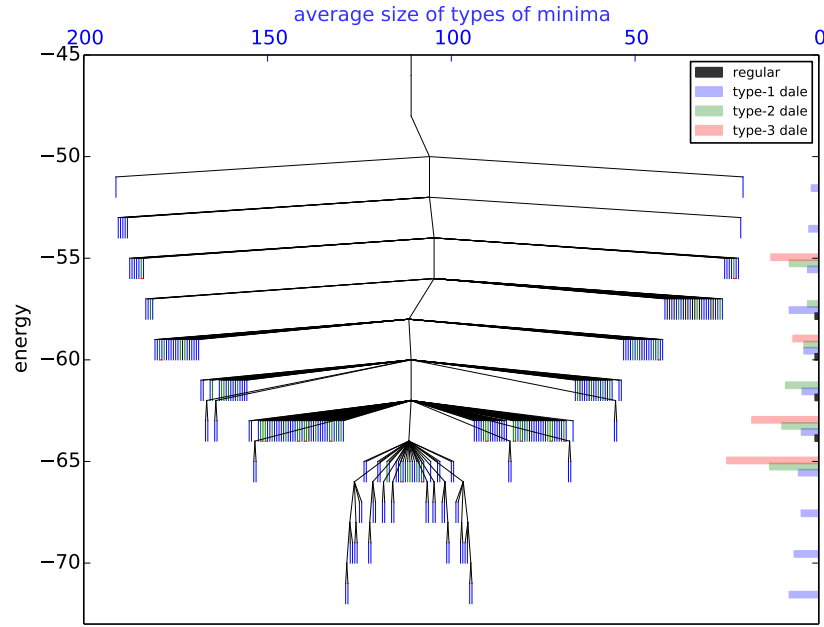


FIG. 8: Example of a disconnectivity graph for a planted spin-glass model (C_2 , see below) on a two-dimensional square lattice with $N = 36$ spins. The black vertical bars represent regular minima, the blue bars represent type-1 dale minima, the green bars represent type-2 dale minima and the red vertical bars indicate type-3 dale minima. The bar chart on the right shows the average size of the types of minima at their respective energy levels. Note, that the axis denoting the average size of types of minima only applies to the bar chart on the right side of the disconnectivity graph.

multiple samples were analyzed, each of which varies in the total number of minima, the normalization is in two steps. First, for each sample separately the distribution of the minimum hamming distance is determined and normalized to unity. Subsequently, an average over samples is performed and the distributions normalized. The standard deviation is computed for the average over samples as are statistically more significant.

As can be seen from Fig. 12, for the three models studied, the shortest hamming distance that occurred most often was 2 with a relative occurrence of 54.7% for C_1 -based models, 81.7% for C_2 -based models, and 95.3% for C_3 -based models. Overall, the C_3 model has a larger number of minima than C_1 and C_2 , see Tab. I. This leads to an overall smaller difference in the orientation of the spins between neighboring minima and therefore shorter hamming distances. Note, that the configuration space consists of all possible combinations of the orientations of the spins of the systems and therefore has the same size for all the three models. This requires the minima of the C_1 model — which on average have fewer minima than C_2 and C_3 — to be more sparsely distributed between the two outermost configurations consisting of either all spins up or all spins down. The remaining minima are distributed between the extreme cases of all spins up and all spins down in model C_1 , thus explaining why there are less states only two spin flips apart than for the other two models, and the rest requiring three (29.4%), four (9.7%), up to a maximum of nine required spin flips between neighboring minima

(0.085%). While these numbers will change with different system sizes, we estimate that the generic trend of the data where two spin flips are dominant remains. The maximum number of required spin flips between neighboring minima for the C_2 model was found to be seven in our sample of 100 systems with an occurrence of 0.018%, and for C_3 it is six at 0.007%.

To verify the validity of our approximation of including only up to 80 barriers for each minimum, we introduce a *barrier field*. The barrier field is the storage allocation of the barriers which are sorted according to their hamming distances, i.e., the hamming distances are sorted according to their size and allocated to the hamming field such that small hamming field values store the information about the barriers for the smallest hamming distances. Figures 13, 14, and 15 show the distribution of the hamming distances for the barrier field for the C_1 , C_2 and the C_3 model systems, respectively. The figures show the results normalized for each value of the barrier field separately and give an indication of the sizes of the hamming distances that are covered by calculating barriers including only 80 neighboring states.

As can be seen from Figs. 13, 14, and 15, in all of the model systems, only a few allocations (i.e., < 10) are necessary to include all the minima within the shortest hamming distance. By obtaining just about 50 barriers for each of the minima hamming distances up to 26 spin flips are covered for the C_1 model system with the highest occurrence of 12 or 13

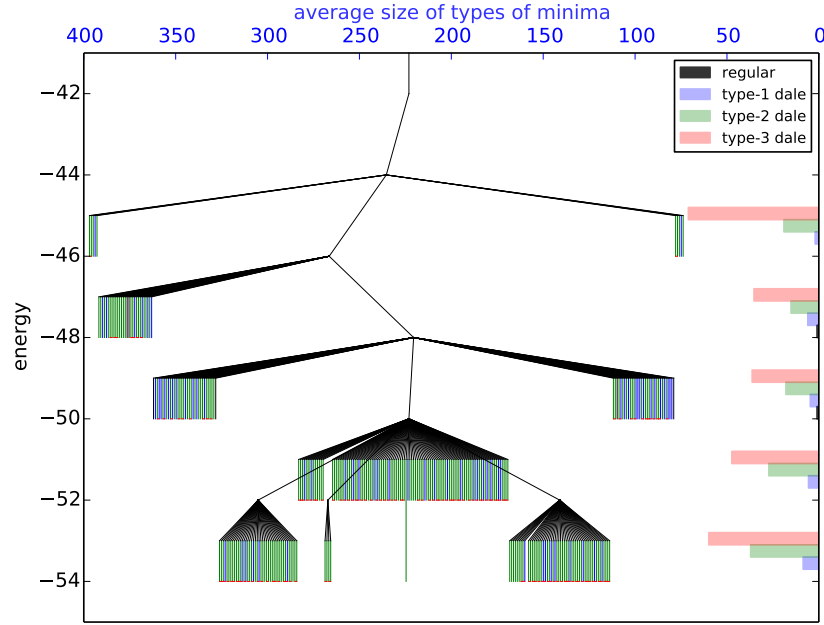


FIG. 9: Example of a disconnectivity graph for a planted spin-glass model (C_3 , see below) on a two-dimensional square lattice with $N = 36$ spins. The black vertical bars represent regular minima, the blue bars represent type-1 dale minima, the green bars represent type-2 dale minima and the red vertical bars indicate type-3 dale minima. The bar chart on the right shows the average size of the types of minima at their respective energy levels. Note, that the axis denoting the average size of types of minima only applies to the bar chart on the right side of the disconnectivity graph.

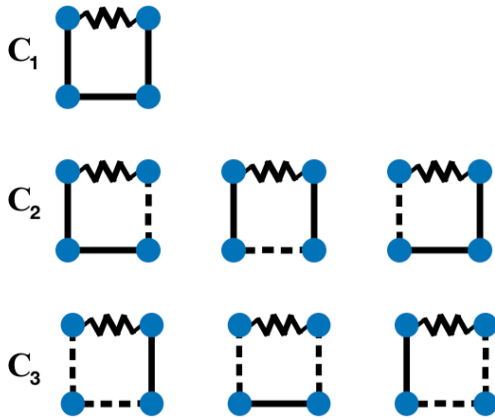


FIG. 10: Schematic representation of the planar unit cells C_1 , C_2 , and C_3 in their invariant form. The solid lines (—) represent $J_{ij} = +2$, the dashed lines (---) represent $J_{ij} = +1$, and the wiggly lines (~~~~) $J_{ij} = -1$.

required flips within the 50th's barrier calculation. For the C_2 model system hamming distances up to 15 occur, with 9 or 10 spin flips having the highest occurrence. For the C_3 model system hamming distances of up to 16 occur, with the highest

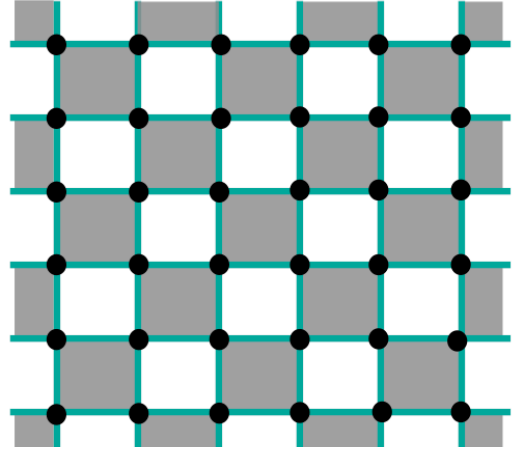


FIG. 11: Schematic representation of the construction pattern of a 6×6 planar system with periodic boundaries. The filled squares represent the tiles in which the unit cells are planted.

occurrence of 7 and 8 necessary flips in the 50 barrier calculation. The difference in the covered hamming distances of the models is due to the difference in the number of minima between the different models, see Tab. I.

Figures 16, 17, and 18 show the distribution of the aver-

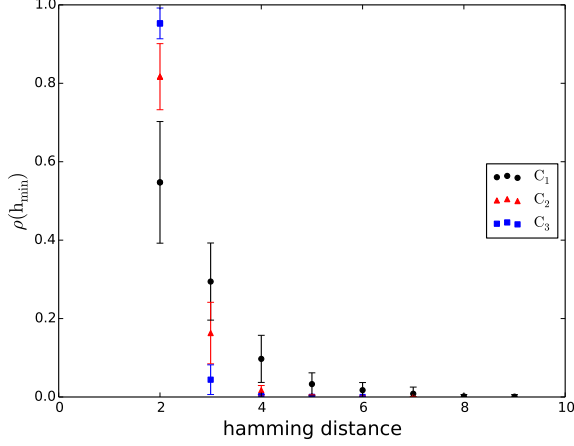


FIG. 12: Distribution of the minimum hamming distance for the C_1 , C_2 , and C_3 models. The vertical bars denote the standard deviation.

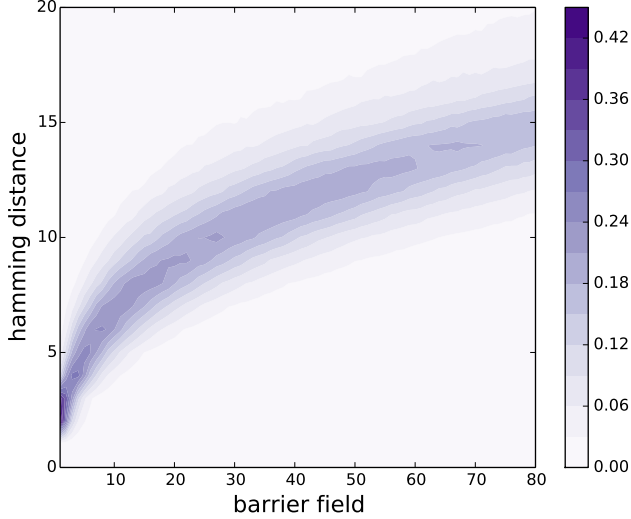


FIG. 13: Distribution of hamming distances vs the barrier field per minima of the C_1 model.

age barrier heights versus the hamming distance of the three model systems C_1 , C_2 , and C_3 . They visualize the calculated range of the barrier field. Note that a dale minimum consists of multiple minima that are joined by zero-energy spin flips, i.e., they form dales on the energy landscape on which the system can transit without an increase in energy. In order to avoid unnecessary double counting, only the barriers corresponding to the shortest hamming distance of minima, belonging to the same dales for type-1 dales and type-2 dales, have been taken into account. Due to the dependence on the pathway, for type-3 dale minima the hamming distance is determined between the endpoints of the individual dales. The figures are normalized to unity for the full distribution.

As can be seen, in all model systems, the barrier heights for

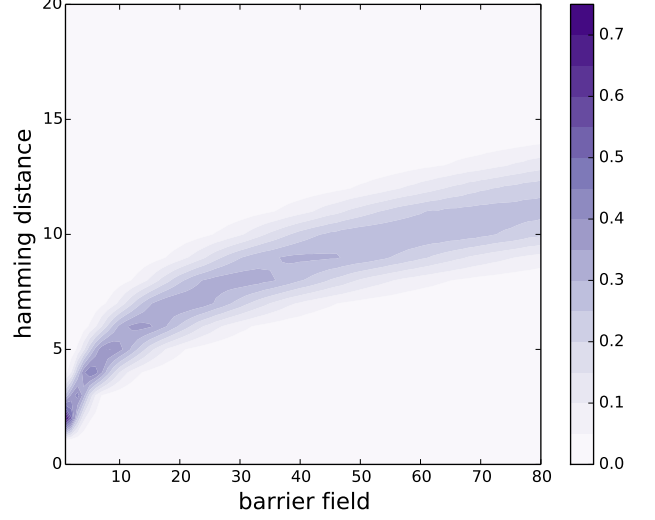


FIG. 14: Distribution of hamming distances vs the barrier field per minima of the C_2 model.

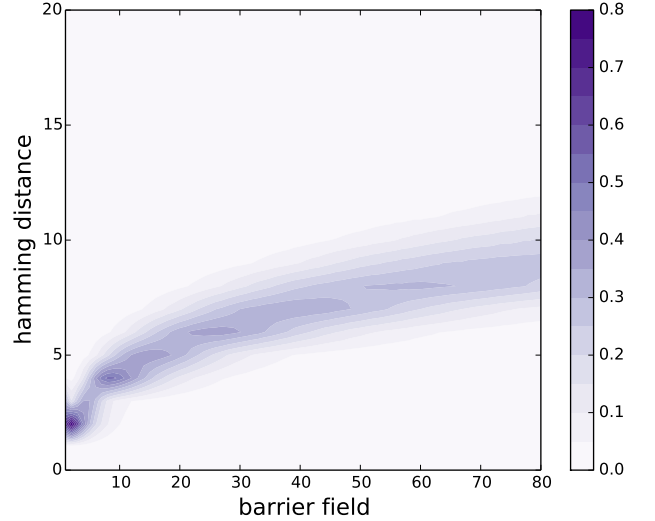


FIG. 15: Distribution of hamming distances vs the barrier field per minima of the C_3 model.

small hamming distances are low. This is due to the fact that when only a few spin flips are necessary to change between minimum energy configurations then only a few spin-spin interactions contribute to the increase in energy of the system. Minima separated by larger hamming distances show a larger distribution of the energy barriers but are also still dominated by small barrier heights. Furthermore, comparing Figs. 16, 17, and 18, a significant contribution of high-energy barriers occurs only at intermediate hamming distances for the model systems C_2 and C_3 . The energy of the highest barrier is larger for C_2 than for C_1 and C_3 , with C_3 having the lowest high barrier. The results from C_3 originate from two factors. First,

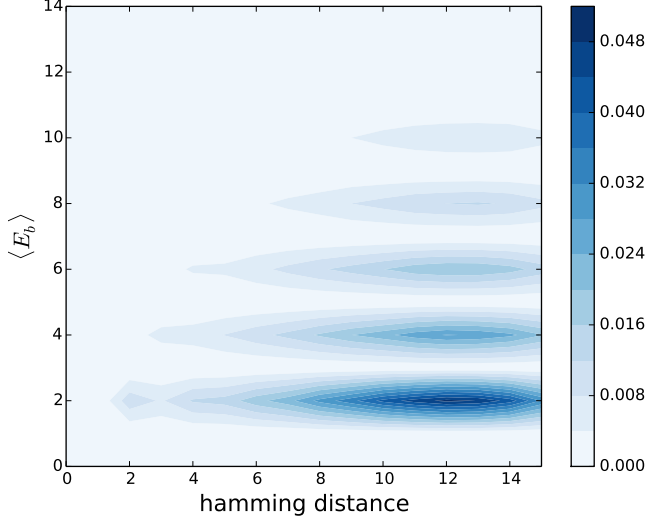


FIG. 16: Distribution of the barrier heights versus the hamming distance for the C_1 model.

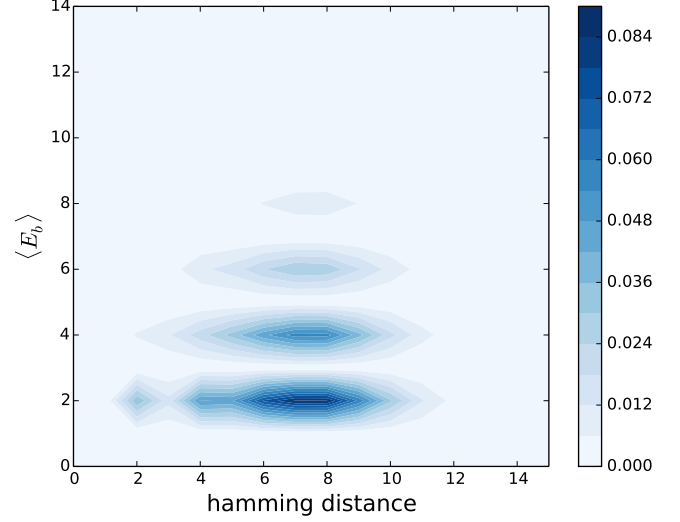


FIG. 18: Distribution of the barrier heights versus the hamming distance for the C_3 model.

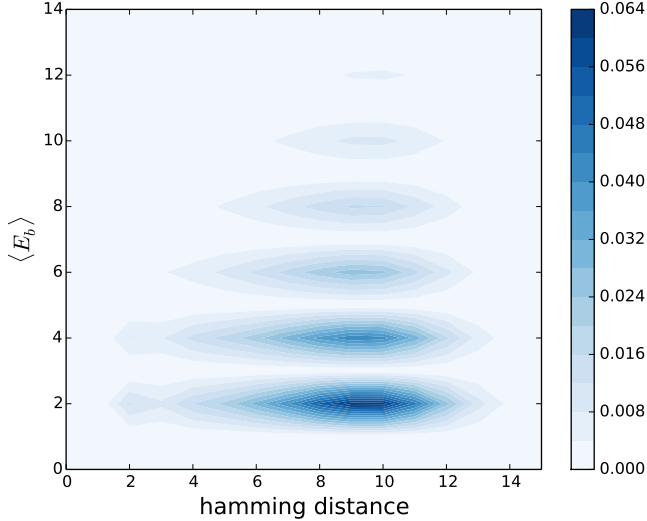


FIG. 17: Distribution of the barrier heights versus the hamming distance for the C_2 model.

due to the large number and huge degeneracy of dale minima in the C_3 model system a larger section of the configuration space is covered than for the other models. Thus, on average a smaller number of spin flips is necessary to traverse between the minima considered in the barrier calculation, also explaining the shorter hamming distances. Second, the C_3 model system has more spin-spin interactions of smaller value than the two other models, which leads to that even if a barrier has to be crossed, the necessary increase in energy between two minima is, in general, smaller than for the other two models. This explains the difference in the observed barrier heights.

These together with the distribution of the hamming dis-

tance for the barrier field (see Figs. 13, 14 and 15) the distribution of the energy barriers confirm with our approximation of the calculation of the barriers. This approximation is based on the assumption that minimum energy transitions between minima, which are far apart on the energy landscape, will most likely occur through pathways that are leading along or through dales of intermediate minima. During such a transition the necessary increase in energy for the total transition will be already captured by intermediate barriers. While low-energy barriers had the highest occurrence indicating the high arrangement of minima into first-order cluster structures, our reduced computation of barriers (i.e., up to a maximum of 80 barriers for each minimum) also covered higher-energy transitions. This allows for transitions out of the local cluster structures. It indicates that for each local cluster there are minima for which the calculated barriers include high-energy transitions, and hence enables the overall connectivity of the minima.

Table I shows the number of minima for the different types of minima of the C_1 , C_2 and the C_3 model system. As can be seen from the table, the actual number of minima \mathcal{N}^* is much higher than the number of minima in the reduced description \mathcal{N} . This is especially striking for the C_3 model, whose energy landscape exhibits a huge number of type-2 dale minima with large sizes of energy dales. The size \mathcal{S} gives the average number of minima belonging to a dale. The average total number of minima, counting each state on a minimum energy dale as individual minimum, is 856.8 for C_1 , 1823.8 for C_2 and 8696.4 for C_3 (post sample average). Especially for C_3 , drawing these huge numbers of minima into disconnectivity graphs would lead to problems. However, using our classification scheme, the average total number of minima in the reduced description is 207.4 for C_1 , 514.2 for C_2 and 774.9 for C_3 , thus making it much simpler to display the energy structure of the minima in the disconnectivity graphs. In

TABLE I: Number of the minima types \mathcal{N} in the reduced description, percentage of the minima $\% \mathcal{N}$ in the reduced description, average size of minima types \mathcal{S} , actual number of minima types \mathcal{N}^* , percentage of the actual number of minima $\% \mathcal{N}^*$. The values are averages obtained from our samples of 100 systems for each of the C_1 , C_2 and C_3 models of tile-planted spin glasses. R denotes regular minima, D1, D2, and D3 denote type-1, type-2, and type-3 minima, respectively [48].

	regular	type-1	type-2	type-3
C_1				
\mathcal{N}	70.7	67.4	69.3	15.3
$\% \mathcal{N}$	34.1	32.5	33.4	
\mathcal{S}	1.0	2.8	8.4	16.8
\mathcal{N}^*	70.7	188.7	582.1	257.0
$\% \mathcal{N}^*$	8.4	22.4	69.2	
C_2				
\mathcal{N}	147.6	238.7	127.9	28.1
$\% \mathcal{N}$	28.7	46.4	24.9	
\mathcal{S}	1.0	3.1	7.1	12.7
\mathcal{N}^*	147.6	740.0	908.1	356.9
$\% \mathcal{N}^*$	8.2	41.2	50.6	
C_3				
\mathcal{N}	61.1	298.6	415.2	102.1
$\% \mathcal{N}$	7.9	38.5	53.6	
\mathcal{S}	1.0	4.8	17.1	30.1
\mathcal{N}^*	61.1	1433.3	7099.9	3073.2
$\% \mathcal{N}^*$	0.7	16.7	82.6	

the reduced description of the minima, in the C_1 model regular minima and type-1 and type-2 minima seem to have equally likely occurred. However, this observation is to be taken with precaution since the reduced description does not take the size of the dales into consideration. Taking the size \mathcal{S} of the minimum energy dales into account, one can see from Tab. I, that most of the individual minimum energy configurations belong to the type-2 minima. Similarly, for the C_2 model, while in the reduced description the number of type-1 minima dominates, taking into account the different sizes \mathcal{S} of the dales shows that the majority of the individual minimum energy configurations belong to the type-2 minima category.

Lastly, compared to the other two model systems, the C_3 model has the smallest percentage of regular minima and the highest percentage of type-2 minima. Together with the high occurrence of low-energy states, this indicates that the energy landscape of this model is easier to traverse using standard optimization routines than the other two models.

Figure 19 shows the average distribution of the energy of the minima E_{\min} in the reduced description and their standard deviation relative to the ground state energy E_{ground} for the three models of tile-planted spin glasses. The large standard deviation in the data is due to the large variation in the number of minima in the generated systems of the three models. As can be seen from Fig. 19 and comparing with the disconnectivity graphs in Figs. 7, 8, and 9, the C_1 model system is distinguished by a large gap between the ground state and higher-order minima. This is not the case for the two other model systems. The majority of the minima of the C_2 model system are found at medium energies, whereas the C_3 model

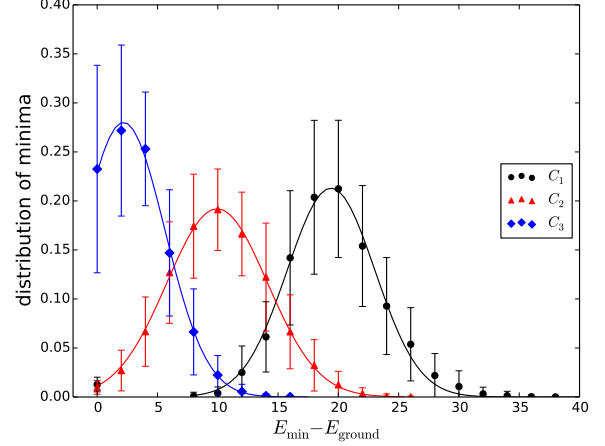


FIG. 19: Distribution of the energy of the minima relative to the energy of the ground state for the different planted spin-glass model systems C_1 (black circles), C_2 (red triangles) and C_3 (blue diamonds). The lines are Gaussian fits and are guides to the eye

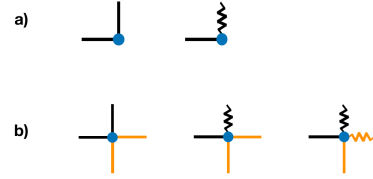


FIG. 20: (a) Possible contributions of spin-spin interactions of an individual C_1 unit cells to a vertex. The solid lines (—) represent $J_{ij} = +2$ spin-spin interactions and the wiggly lines (⋯) $J_{ij} = -1$ spin-spin interactions. (b) Possible combinations of the spin-spin interactions to a vertex of model system C_1 . No zero-energy spins are possible if all neighboring spins point in the same direction.

is distinguished by a large number of minima energetically close to the ground state.

Figures 7, 8 and 9 show examples of the disconnectivity graphs of the C_1 , C_2 , and the C_3 model systems, respectively. As can be seen from Fig. 7 (see also Fig. 21), the ground state of the C_1 model system has an energy of $E_{\text{ground}} = -90$. This is due to the fact that each unit cell has an energy of $H = -5$ corresponding to a configuration in which either all spins are up or all spins are down and there are 18 unit cells in the lattice studied. Furthermore, the ground state of the C_1 model system is always a regular minimum. Figure 20(a) shows the possible combinations of spin-spin interactions to a vertex belonging to a single unit cell. Each unit cell can contribute to a vertex either two $J_{ij} = +2$ or one $J_{ij} = +2$ and one $J_{ij} = -1$ spin-spin interaction. Since two unit cells join at each vertex, this gives the possible combinations of spin-spin interactions shown in Fig. 20(b). As can be seen, none of the possible combinations of spin-spin interactions leads to a zero-energy vertex if all neighboring spins have the same orientation. Hence, the ground states of the C_1 model are always regular minima.

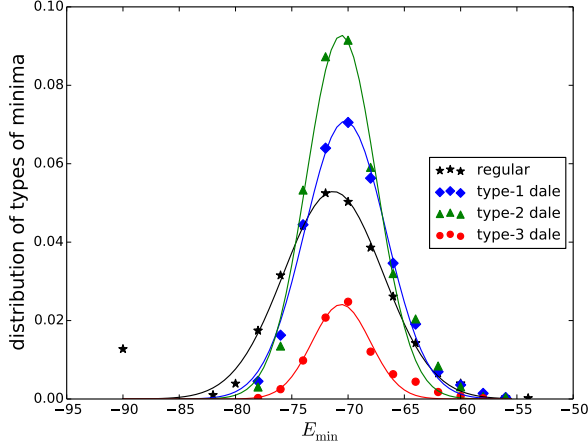


FIG. 21: Distribution of the different dale minima types for the C_1 model system of planted spin glasses. The lines are Gaussian fits and guides to the eye [49].

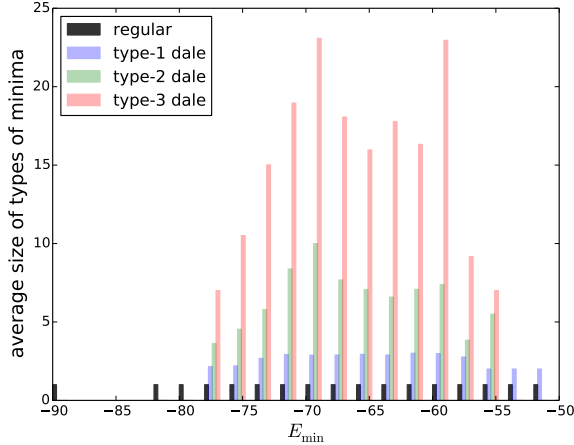


FIG. 22: Average size of the different dale minima types for the C_1 model of planted spin glasses.

Figure 21 shows the distribution of the minima types of the C_1 model system for all the minima. One can see in Fig. 21 that the ground states of this model are always regular minima and are separated by a large energy gap to higher energy states. It appears that the C_1 model system has on average the highest number of states belonging to type-2 dale minima (see Tab. I). This suggests that with a simple optimization routine one is most likely to encounter type-2 dale minima lying in the median regions of the energetically possible configurations.

Figure 22 shows the average size of the minima and types of dale minima at their respective energies. With size we understand here the number of subminima that make up the different types of dales. Regular minima consist of only one subminimum, hence their size is always one at any energy level on which they occur. The size of the different types of dales is always larger than that of the regular minimum, with

type-3 dales having the highest number of subminima because these are composed of two dales of type-1 or type-2 joined together. The occurrence that type-1 dale minima are smaller than type-2 dale minima at all energy levels (Fig. 22) is not a general property of the types of dales. It is a specific feature of the model studied. Furthermore, as can be seen from Fig. 22, the number of subminima belonging to the individual dales is especially large around medium energies (at about $E_{\min} = -70$) with a second peak at $E_{\min} = -60$. Taking into account the findings of the distribution of the types of minima (Fig. 21) only the first peak considerably contributes to the features of the energy landscape. The second peak, while comparably large in the size of type-2 and type-3 dale minima, has a low occurrence (less than 0.01, see Fig. 21) and thus has little significance for general optimization procedures. The size of type-1 dale minima does not vary much and is always less than four for the system sizes studied.

The ground states of the C_2 model are either regular minima or type-1 dale minima and have a ground-state energy of $E_{\text{ground}} = -72$, because each of the 18 cells has an energy of $H = -4$. For the planted ground-state solutions the occurrence of type-1 dale minima can be understood by considering the possible combinations of spin-spin interactions to the spins. Figure 23 illustrates this situation. The possible contributions of spin-spin interactions of a single unit cell to a vertex are shown in Fig. 23(a). In Fig. 23(b) the possible distinct combinations of spin-spin interactions to a vertex are shown. Only one of these combinations allows for a zero-energy spin in the planted solutions, i.e., two unit cells need to be oriented in such a way, that from each of the cells one $J_{ij} = +1$ and one $J_{ij} = -1$ spin-spin interaction join at the vertex. Only then the energy of the vertex will be balanced if all neighboring spins point in the same direction. However, because each of the two unit cells already contributes with their $J_{ij} = +1$ and $J_{ij} = -1$ spin-spin interactions, the remaining spin-spin interactions of each of the two unit cells are $J_{ij} = +2$ as illustrated in Fig. 23. This makes it impossible for any of the neighboring vertices to the zero-energy vertex to be energetically balanced in the planted solution. This prohibits the formation of connected zero-energy spins, and hence the planted solutions of this model will always be regular minima or type-1 dale minima.

Figure 24 shows the distribution of minima types in the reduced description of all the minima in the C_2 model. Different to the C_1 model system, the C_2 model does not have a large gap to the ground state. Similarly to C_1 , the majority of the minima populate the energetically medium regions. Together with the higher number of minima, this suggests that this type will be harder to solve in optimization routines than C_1 and C_3 . This was also observed in the study of Perera *et al.* [38], which compares the time to solution of different models of tile-planted spin glasses.

Figure 25 shows the average size of the types of minima at their respective energies. The size of types of minima follows the same order as in the C_1 model, with regular minima always having size one, followed by type-1 dale minima, type-2 dale minima, and type-3 dale minima having the largest size. In contrast to C_1 in the C_2 model, no distinct peak in the size

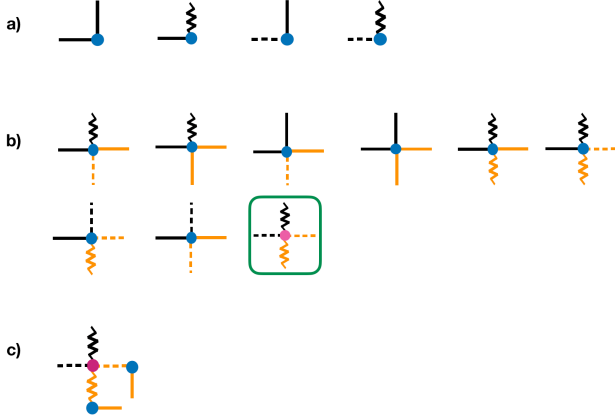


FIG. 23: (a) Possible contributions of spin-spin interactions of a single C_2 unit cell to a vertex. The bonds $J_{ij} = -1, 1$, and 2 are indicated by wiggly lines (\sim), dashed lines ($---$), and solid lines ($—$) respectively. (b) Possible combinations of the spin-spin interactions to a vertex of model system C_2 . Only one of the combinations (framed) allows for zero-energy spins for the planted solutions. (c) The zero-energy vertex of case (b) only leaves $J_{ij} = +2$ spin-spin interactions for each joining unit cell, hence this system cannot have neighboring zero-energy spins in the planted solution.

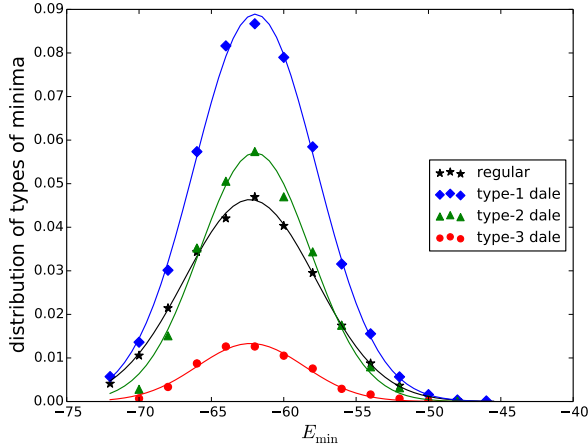


FIG. 24: Distribution of the different dale type minima for the C_2 model of planted spin glasses. The lines are Gaussian fits and guides to the eye [49].

is visible. The largest sizes of the dales seem to span a range from $E_{\min} = -66$ to $E_{\min} = -54$ for the system size studied. However, taking into account the high occurrence of dales at the energy of $E_{\min} = -62$ (see Fig. 24) indicates that especially energies in this range have on average the highest number of states pertaining to minimum energy configurations.

Figure 9 shows an example of the disconnectivity graph for the C_3 model. Due to the small values of the spin-spin interactions, the ground state of the C_3 model is highly degenerate. It exhibits a large number of minima of all types and has the energy $E_{\text{ground}} = -54$ as each of the 18 cells has an energy of

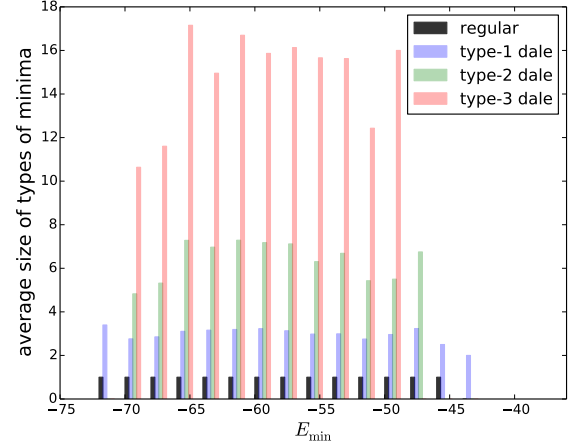
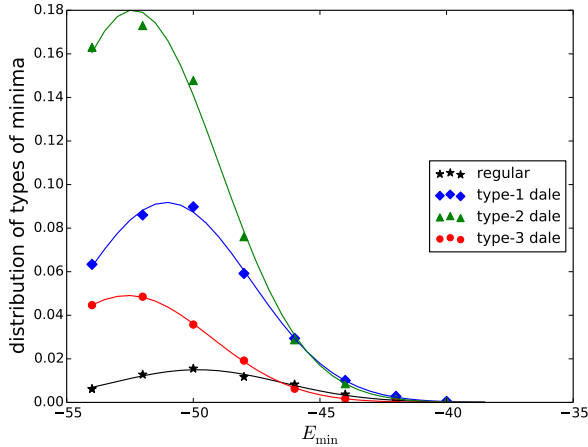
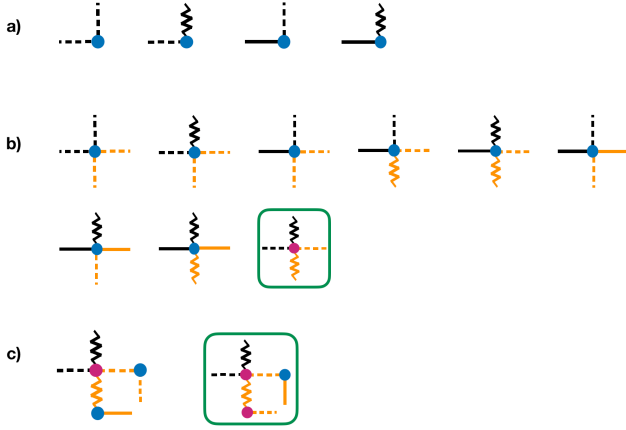


FIG. 25: Average size of the different dale minima types for the C_2 model of planted spin glasses.

$H = -3$. Figure 26 (a) shows the possible contributions of the spin-spin interactions of a single unit cell to a vertex. If two unit cells are joined at a vertex, the possible distinct combinations of spin-spin interactions to a vertex are shown in Fig. 26. Note that from these combinations, similar to the C_2 model system, only one configuration of spin-spin interactions leads to a zero-energy spin. This combination is framed in green in the figure. However, different from the C_2 case, it allows for larger structures of connected zero-energy spins (see Fig. 26). These connected structures allow for type-2 dale minima and since the spin-spin interactions to spins that are connected to zero-energy spins can be balanced once the zero-energy spins have been flipped, this allows also for type-3 dale minima to occur. Hence, the planted solutions of model system C_3 can be regular minima or dale-minima of any type.

Figure 27 shows the distribution of the minima types in the reduced description of the C_3 model system. Different to the C_1 and C_2 model systems, a large number of minima is energetically close to the ground state. This model is dominated by type-2 dale minima suggesting the formation of large minimum-energy dales on the energy landscape, i.e., on average each dale consists of 17 individual configurations connected by zero-energy spins (see Tab. I). Furthermore, this model has the least number of regular minima at any energy. These results suggest that, using standard optimization procedures, a configuration belonging to the ground state will be easier to find for the C_3 model than for the other models. This is in agreement with the numerical results of Perera *et al.* [38].

Figure 28 shows the average size of the types of minima at their respective energies of the C_3 model. As can be seen, similar to the C_1 and C_2 model, regular minima always have size one, i.e., they consist of only one subminimum, and type-3 dale minima have the largest number of subminima. However, different from both the C_1 and C_2 models, type-2 dale minima are not always larger than type-1, i.e., only for energies up to $E_{\min} = -38$ the type-2 dale minima consist of more subminima than the type-1 dale minima, but at the high-



est occupied energy level at $E_{\min} = -36$ type-1 dale minima are on average larger than type-2 dales. The size of type-1 dale minima is relatively constant (≤ 5) for all energy levels. Type-2 and type-3 dales are largest at the lowest energies, which together with their very high occurrence (compare to Fig. 27) is a further indication of the relative ease at which lowest-energy states can be found.

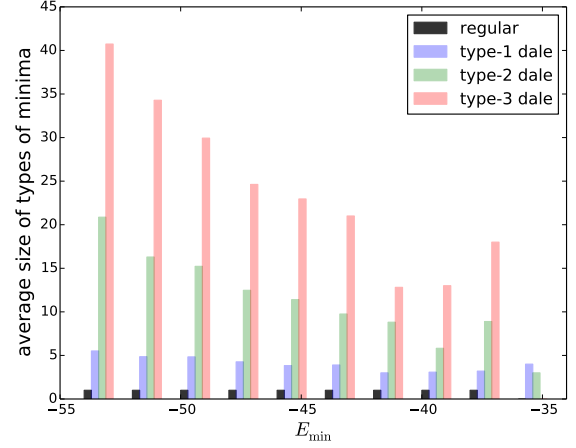


FIG. 28: Average size of the different dale types for the C_3 model system of planted spin glasses.

V. SUMMARY

We introduce a classification scheme for the different types of connected degenerate minima, which we call dale minima. We distinguish between regular minima, i.e., minima for which a flip of any spin would increase the energy, and dale minima. The dale minima form broad valleys in the energy landscape and are composed of multiple minima connected via zero-energy spin flips. We distinguish between three different types of dale minima based on similarity and accessibility of the states to each other. This procedure effectively helps to reduce the number of stored minima during the computation and eases the visualization of disconnectivity graphs. In the disconnectivity graphs, the dale minima are distinguished by colors. Furthermore, we add a bar chart depicting the average number of subminima pertaining to the dales at the respective energy levels. The added classification into different types of minima allows for an enhanced version of disconnectivity graphs that give an intuitive understanding of the important aspects of the potential energy landscape of spin systems.

We apply our classification scheme to a spin-glass model with planted solutions and differentiate between the three elementary problem classes, namely C_1 , C_2 , and C_3 . The resulting disconnectivity graphs and subsequent analysis show distinctly different features for the different classes. C_1 systems only have two ground states, corresponding to the ferromagnetic solution of all spins up or all spins down. Its higher-energy states are separated by a large gap to the ground state and are highly degenerate. All of the states, including the ground states, of the C_2 and C_3 model systems are degenerate, but do not have a large gap to the ground-state. Compared to C_1 and C_2 , C_3 instances have the highest number of ground-states relative to higher energy states, leading us to conclude that C_3 instances are the easiest to solve when using conventional optimization routines. Plots of the different minima types versus their energy show distinct Gaussian features, with the mean of the C_1 and C_2 models being centered

at energies above the ground state. Only for C_3 instances are the majority of the minima located close to the ground state.

While our analysis of these types of planted spin glasses is limited to a system size of 36 spins, we estimate that the general features of the energy landscape, such as the occurrence of ground-state solutions and the relative distribution of the minima across different energy levels, is preserved for larger system sizes. Similar arguments hold for the occurrence of the different types of states and their distribution over the different energy levels. Note, however, that our conclusions are based on relatively small system sizes because the phase space grows exponentially with the number of spins. This means that further types of states might occur when the system sizes are increased. However, the developed methods can be generally applied, thus presenting a simple visual approach to characterize the phase space of statistical mechanical systems.

Acknowledgments

We would like to thank Dilina Perera for feedback on the manuscript. H.G.K. would like to thank Izumi Kirkland for in-

spiration. This research is based upon work supported in part by the Office of the Director of National Intelligence (ODNI), Intelligence Advanced Research Projects Activity (IARPA), via MIT Lincoln Laboratory Air Force Contract No. FA8721-05-C-0002. The views and conclusions contained herein are those of the authors and should not be interpreted as necessarily representing the official policies or endorsements, either expressed or implied, of ODNI, IARPA, or the U.S. Government. The U.S. Government is authorized to reproduce and distribute reprints for Governmental purpose notwithstanding any copyright annotation thereon. We thank the Texas A&M University for providing high performance computing resources.

-
- [1] O. M. Becker and M. Karplus, *The topology of multidimensional potential energy surfaces: Theory and application to peptide structure and kinetics*, J. Chem. Phys. **106**, 1495 (1997).
 - [2] C. L. Brooks, J. N. Onuchic, and D. J. Wales, *Taking a Walk on a Landscape*, Science **293**, 612 (2001).
 - [3] D. Wales, *Energy Landscapes: Applications to Clusters, Biomolecules and Glasses* (Cambridge University Press, Cambridge, 2004).
 - [4] D. J. Wales, *Energy landscapes and properties of biomolecules*, Physical Biology **2**, S86 (2005).
 - [5] Z. Wang, A. Marandi, K. Wen, R. L. Byer, and Y. Yamamoto, *Coherent Ising machine based on degenerate optical parametric oscillators*, Phys. Rev. A **88**, 063853 (2013).
 - [6] S. V. Isakov, I. N. Zintchenko, T. F. Rønnow, and M. Troyer, *Optimized simulated annealing for Ising spin glasses*, Comput. Phys. Commun. **192**, 265 (2015), (see also ancillary material to arxiv:cond-mat/1401.1084).
 - [7] S. Tsukamoto, M. Takatsu, S. Matsubara, and H. Tamura, *An Accelerator Architecture for Combinatorial Optimization Problems*, FUJITSU Sci. Tech. J. **53**, 8 (2017).
 - [8] S. Matsubara, H. Tamura, M. Takatsu, D. Yoo, B. Vatanhahghadim, H. Yamasaki, T. Miyazawa, S. Tsukamoto, Y. Watanabe, K. Takemoto, et al., in *Complex, Intelligent, and Software Intensive Systems – Proceedings of the 11th International Conference on Complex, Intelligent, and Software Intensive Systems (CISIS-2017), Torino, Italy, July 10–12, 2017* (2017), p. 432.
 - [9] M. Aramon, G. Rosenberg, T. Miyazawa, H. Tamura, and H. G. Katzgraber, *Physics-inspired optimization for constraint-satisfaction problems using a digital annealer*, Front. Phys. **7**, 48 (2019).
 - [10] R. Hamerly, T. Inagaki, P. L. McMahon, D. Venturelli, A. Marandi, T. Onodera, E. Ng, C. Langrock, K. Inaba, T. Honjo, et al., *Experimental investigation of performance differences between coherent Ising machines and a quantum annealer*, Sci. Adv. **5**, eaau0823 (2019).
 - [11] T. F. Rønnow, Z. Wang, J. Job, S. Boixo, S. V. Isakov, D. Wecker, J. M. Martinis, D. A. Lidar, and M. Troyer, *Defining and detecting quantum speedup*, Science **345**, 420 (2014).
 - [12] B. Heim, T. F. Rønnow, S. V. Isakov, and M. Troyer, *Quantum versus classical annealing of Ising spin glasses*, Science **348**, 215 (2015).
 - [13] I. Hen, J. Job, T. Albash, T. F. Rønnow, M. Troyer, and D. A. Lidar, *Probing for quantum speedup in spin-glass problems with planted solutions*, Phys. Rev. A **92**, 042325 (2015).
 - [14] S. Mandrà, Z. Zhu, W. Wang, A. Perdomo-Ortiz, and H. G. Katzgraber, *Strengths and weaknesses of weak-strong cluster problems: A detailed overview of state-of-the-art classical heuristics versus quantum approaches*, Phys. Rev. A **94**, 022337 (2016).
 - [15] S. Mandrà and H. G. Katzgraber, *The pitfalls of planar spin-glass benchmarks: Raising the bar for quantum annealers (again)*, Quantum Sci. Technol. **2**, 038501 (2017).
 - [16] S. Mandrà and H. G. Katzgraber, *A deceptive step towards quantum speedup detection*, Quantum Sci. Technol. **3**, 04LT01 (2018).
 - [17] G. Toulouse, *Theory of the frustration effect in spin glasses*, Commun. Phys. **2**, 115 (1977).
 - [18] S. Kirkpatrick, *Frustration and ground-state degeneracy in spin glasses*, Phys. Rev. B **16**, 4630 (1977).
 - [19] P. W. Anderson, *The concept of frustration in spin glasses*, Journal of the Less Common Metals **62**, 291 (1978).
 - [20] P. Garstecki, T. X. Hoang, and M. Cieplak, *Energy landscapes, supergraphs, and “folding funnels” in spin systems*, Phys. Rev. E **60**, 3219 (1999).
 - [21] C. Amoruso, A. K. Hartmann, and M. A. Moore, *Determining Energy Barriers by Iterated Optimization: The Two-Dimensional Ising Spin Glass*, Phys. Rev. B **73**, 184405 (2006).
 - [22] Z. Burda, A. Krzywicki, O. C. Martin, and Z. Tabor, *From simple to complex networks: Inherent structures, barriers, and val-*

- leys in the context of spin glasses, *Phys. Rev. E* **73**, 036110 (2006).
- [23] Z. Burda, A. Krzywicki, and O. C. Martin, *Network of inherent structures in spin glasses: Scaling and scale-free distributions*, *Phys. Rev. E* **76**, 051107 (2007).
- [24] J. Krawczyk and S. Kobe, *Low-temperature dynamics of spin glasses: walking in the energy landscape*, *Physica A* **315**, 302 (2002).
- [25] J. Dall and P. Sibani, *Exploring valleys of aging systems: the spin glass case*, *Eur. Phys. J. B* **36**, 233 (2003).
- [26] J. F. Fontanari and P. F. Stadler, *Fractal geometry of spin-glass models*, *J. Phys. A* **35**, 1509 (2002).
- [27] W. Hordijk, J. F. Fontanari, and P. F. Stadler, *Shapes of tree representations of spin-glass landscapes*, *J. Phys. A* **36**, 3671 (2003).
- [28] H. Seyed-allaei, H. Seyed-allaei, and M. R. Ejtehadi, *Energy-landscape networks of spin glasses*, *Phys. Rev. E* **77**, 031105 (2008).
- [29] Q. Zhou and W. H. Wong, *Energy landscape of a spin-glass model: Exploration and characterization*, *Phys. Rev. E* **79**, 051117 (2009).
- [30] Q. Zhou, *Random Walk over Basins of Attraction to Construct Ising Energy Landscapes*, *Phys. Rev. Lett.* **106**, 180602 (2011).
- [31] These dales are sometimes also referred to as U-shaped minima [20], clusters [24, 32–35], or local ensembles of ground states.
- [32] A. K. Hartmann, *A new method for analysing ground-state landscapes: ballistic search*, *J. Phys. A* **33**, 657 (2000).
- [33] A. K. Hartmann, *Ground-state clusters of two-, three-, and four-dimensional $\pm J$ Ising spin glasses*, *Phys. Rev. E* **63**, 016106 (2000).
- [34] A. K. Hartmann and A. P. Young, *Large-scale low-energy excitations in the two-dimensional Ising spin glass*, *Phys. Rev. B* **66**, 094419 (2002).
- [35] A. Mann and A. K. Hartmann, *Numerical solution-space analysis of satisfiability problems*, *Phys. Rev. E* **82**, 056702 (2010).
- [36] J. W. Landry and S. N. Coppersmith, *Ground states of two-dimensional $\pm J$ Edwards-Anderson spin glasses*, *Phys. Rev. B* **65**, 134404 (2002).
- [37] F. Hamze, D. C. Jacob, A. J. Ochoa, D. Perera, W. Wang, and H. G. Katzgraber, *From near to eternity: Spin-glass planting, tiling puzzles, and constraint-satisfaction problems*, *Phys. Rev. E* **97**, 043303 (2018).
- [38] D. Perera, F. Hamze, J. Raymond, M. Weigel, and H. G. Katzgraber, *Computational hardness of spin-glass problems with tile-planted solutions*, *Phys. Rev. E* **101**, 023316 (2020).
- [39] V. Martin-Mayor and I. Hen, *Unraveling Quantum Annealers using Classical Hardness* (2015), (arXiv:1502.02494).
- [40] H. G. Katzgraber, F. Hamze, and R. S. Andrist, *Glassy Chimeras Could Be Blind to Quantum Speedup: Designing Better Benchmarks for Quantum Annealing Machines*, *Phys. Rev. X* **4**, 021008 (2014).
- [41] H. G. Katzgraber, F. Hamze, Z. Zhu, A. J. Ochoa, and H. Munoz-Bauza, *Seeking Quantum Speedup Through Spin Glasses: The Good, the Bad, and the Ugly*, *Phys. Rev. X* **5**, 031026 (2015).
- [42] J. Marshall, V. Martin-Mayor, and I. Hen, *Practical engineering of hard spin-glass instances*, *Phys. Rev. A* **94**, 012320 (2016).
- [43] W. Wang, S. Mandrà, and H. G. Katzgraber, *Patch-planting spin-glass solution for benchmarking*, *Phys. Rev. E* **96**, 023312 (2017).
- [44] We use the word dale to highlight the discrete nature of the energies of our systems.
- [45] Barriers between any two minima for all the minima in the system.
- [46] Y. Levy and O. M. Becker, *Effect of Conformational Constraints on the Topography of Complex Potential Energy Surfaces*, *Phys. Rev. Lett.* **81**, 1126 (1998).
- [47] One would expect the overall structure of the cluster to be highly symmetric due to the symmetry regarding a flip of all spins of the individual minima. This, however, is a feature of the highly multi-dimensional nature of the energy landscape and can only be hinted at in two-dimensional representations.
- [48] Note, that since type-3 dale minima consist of type-1 and type-2 dale minima, which are joined by directional paths, the values given in this column relate only to the total number of minima, but not to the other types. They are to be interpreted separately.
- [49] Note that type-3 dales consist of type-1 and type-2 dales joined together. In order to avoid double counting, this figure is normalized to unity taking into account only regular minima, type-1, and type-2 dales. The values for type-3 dales are with respect to the total number of minima of the systems.